

The Saturn Target for Polar Direct Drive on the National Ignition Facility

R. S. Craxton* and D. W. Jacobs-Perkins

Laboratory for Laser Energetics, University of Rochester, 250 East River Road, Rochester, New York 14623-1299, USA
(Received 18 November 2004; published 9 March 2005)

A new target design concept is proposed for direct-drive implosions while the National Ignition Facility is in its initial, indirect-drive configuration. It differs from earlier “polar-direct-drive” designs by adding a low-Z ring around the capsule equator. Refraction in the plasma formed around this ring permits time-dependent tuning of the capsule drive uniformity. An optimized simulation shows an implosion-velocity nonuniformity at the end of the laser pulse of $\sim 1\%$ rms for a cryogenic deuterium-tritium shell, enhancing the prospects for an early direct-drive ignition demonstration on the National Ignition Facility.

DOI: 10.1103/PhysRevLett.94.095002

PACS numbers: 52.57.Fg, 52.57.Bc

Direct-drive illumination plays a significant role in plans to achieve ignition on the National Ignition Facility (NIF) [1]. Ignition requires the uniform implosion of a fuel capsule containing a deuterium-tritium (DT) mixture with intense laser beams, using either direct laser illumination of the capsule [2] or indirect drive [3], in which laser beams focused into a hohlraum generate x rays to drive the capsule. The baseline NIF target chamber geometry requires that all the NIF beams be incident through 48 beam ports, known as the “indirect-drive” ports, located in rings with angles varying from 23.5° to 50° with respect to the vertical (pole). Additional beam ports near the equator, at an angle of 77.45° , allow symmetric direct-drive illumination to be accommodated at a later time by rerouting half of the beams to these ports [4]. Considerable interest has been stimulated by the recent reconsideration [5–7] of direct drive using the indirect-drive ports with the beams repointed toward the equator, a concept now known as polar direct drive (PDD) [5]. PDD may allow direct-drive ignition and possibly high gain to be achieved on the NIF many years earlier than would otherwise be possible.

This Letter reports a new PDD target design concept that promises to improve the drive uniformity on the capsule compared with the previous (“standard-PDD”) designs of Refs. [5–7]. The new “Saturn” design, whose distinctive feature is a low-Z ring placed in the equatorial plane of the capsule (Fig. 1), is applied to the “all-DT” design of Refs. [8,9]. The Saturn design can result in a DT shell that is imploding at the end of the laser pulse with a velocity uniform to a little over 1% (rms), close to the uniformity expected for the “symmetric” design that uses the direct-drive ports with all beams pointed to the capsule center [9].

The primary limitation on the uniformity attainable with standard PDD arises because extra laser power needs to be focused near the equator to compensate for the oblique angle of incidence, but the radius of the critical surface (near which most absorption occurs) decreases significantly during the laser pulse. Since the NIF laser beams cannot be dynamically repointed, two methods have hitherto been proposed to minimize this effect: careful opti-

mization of the beam pointings [5–7] and the use of different pulse shapes for the different rings of beams [5]. The essence of the Saturn design is that a plasma forms around the low-Z ring, from laser rays refracted from the capsule plasma and from rays on the edges of Ring-4 beams (those incident at 50° in Fig. 1) that clip the low-Z ring. The ring plasma has little impact on the capsule irradiation pattern at early times, but later expands into the path of a significant portion of Ring-4 rays, deflecting them to strike the imploding critical surface near the equator. Optimum designs match the expansion of the ring plasma to the implosion of the capsule plasma.

Figure 1 gives the main parameters of the Saturn design. Three of the four rings of beams in each hemisphere (the lower-hemisphere beams are not shown) are repointed toward the equator with the specified distances Δr measured perpendicular to the beam axes. Rings 3 and 4 use “elliptical phase plates,” whose focal spot is shortened in the vertical direction by a factor of $\cos\theta_{pp}$. Prior to this

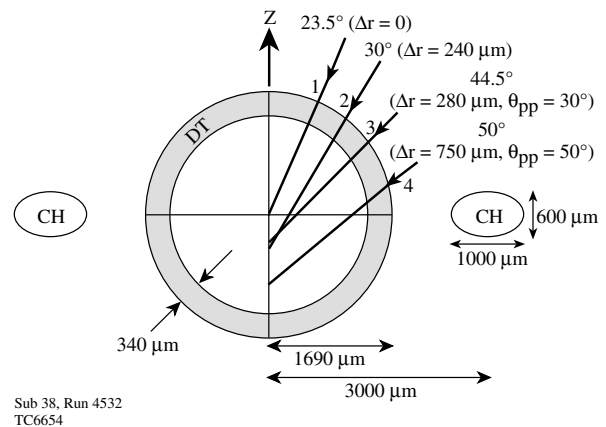


FIG. 1. Vertical cross section of a Saturn target for direct drive on the NIF. The capsule (the all-DT design of Ref. [9]) is a $340\ \mu\text{m}$ layer of cryogenic DT supported in a thin (few μm) plastic shell. It is irradiated using the four rings of indirect-drive ports in each hemisphere and the indicated repointings. The capsule is surrounded by a low-Z (CH) ring whose plasma provides time-dependent pointing correction for Ring-4 beams.

shortening, all beams have super-Gaussian target-plane spatial shapes with the intensity proportional to $\exp-(r/r_0)^{2.5}$ with $r_0 = 1200 \mu\text{m}$. The capsule is a thick shell ($340 \mu\text{m}$) of cryogenic DT ice contained within a thin (few μm) plastic shell of outer radius $1690 \mu\text{m}$ [9]. The low-Z ring, made of CH to minimize radiation preheat, has a major radius R_{major} of $3000 \mu\text{m}$ and an elliptical cross section. While the parameters listed in Fig. 1 were selected as a result of numerous two-dimensional (2D) simulations, improvements are likely because of the large range of possible parametric variations.

The Saturn design is compared with standard-PDD and symmetric designs obtained using similar optimizations and the same super-Gaussian profiles. The pointings used for standard PDD are $\Delta r = 100, 290, 380,$ and $750 \mu\text{m}$, respectively, for Rings 1–4 and $\theta_{pp} = 30^\circ$ and 60° , respectively, for Rings 3 and 4 (as in Ref. [7]).

The target is irradiated by the incident laser temporal pulse shape taken from Ref. [9] and shown in Fig. 2 as the upper curve. The total incident energy is 1.53 MJ, less than the nominal total NIF energy [1] of 1.8 MJ. All beams have the same power history, maximizing the available on-target energy. The other curves in Fig. 2 give the absorbed laser power for the three cases. The overall absorption for standard PDD (63%) is only slightly less than the 66% of the

symmetric case because the elliptical phase plates compensate for the absorption loss of the repointed beams. The Fig. 2 inset shows the elliptical 10% intensity contour (the outer ellipse) in the target plane of a Ring-4 beam pointed $750 \mu\text{m}$ below the target center together with the initial and final critical-surface radii. The Saturn capsule absorbs slightly more (70%), and just under half of the energy refracted from the capsule is absorbed in the CH ring (bottom curve).

The simulations reported here used the 2D Eulerian hydrodynamics code SAGE, which includes fully self-consistent, 3D laser ray tracing [10]. Each of the eight rings (four per hemisphere) is represented by a single beam whose incoming cross section is broken into a grid of ~ 1000 rays (shown schematically in the Fig. 2 inset). Each ray is traced through an (x, y, z) coordinate system, with z vertical, and the energy at each step is deposited by inverse bremsstrahlung onto the spherical (r, θ) simulation grid at radius $r = (x^2 + y^2)^{1/2}$. This is equivalent to averaging the deposited energy in the azimuthal (ϕ) direction. The azimuthal variations due to the finite number of beams in each NIF ring are expected to be smaller than the variations in θ due to the PDD geometry.

Typical plots of density contours and ray trajectories [projected into the (r, θ) plane] are shown in Fig. 3 for the Saturn and standard-PDD cases, at 5.8 ns (close to the time that the initial shock reaches the inner DT surface) and at 9 ns (roughly the end of the laser pulse). For clarity, only a small fraction of the Ring-4 rays are shown. At 5.8 ns, the plasma forming around the CH ring is not large enough to significantly deflect the central rays (marked with arrows). At 9 ns, however, significant refraction of the central group of rays toward the capsule equator is evident in the Saturn case, while these rays pass significantly below the equator in the standard-PDD case. An additional effect included in the simulations is tamping of the blowoff by the CH ring that may also enhance the pressure near the equator.

The deviations of the center-of-mass radius and radial velocity (V_r) of the imploding shell at 9 ns are shown in Fig. 4 for the three cases. The standard-PDD case shows significant structure, in particular, a large radius and small velocity near the equator. The Saturn case reduces the rms velocity variation to 1.3%, close to the 1.0% predicted for the symmetric case. A uniform V_r is critical to a uniform implosion, and the target designs were chosen to minimize the rms of this quantity. The quoted rms values are probably upper bounds since the simulations, which should be symmetric about $\theta = 90^\circ$, include some numerical noise. The Saturn-design V_r nonuniformity is dominated by Legendre modes $\ell = 2$ and 4 (1.1% in these modes), with the other 0.2% attributable to noise. The predominantly low- ℓ content in the Saturn case provides a significant advantage compared with the standard-PDD case, as the all-DT capsule design is more tolerant of low- ℓ modes

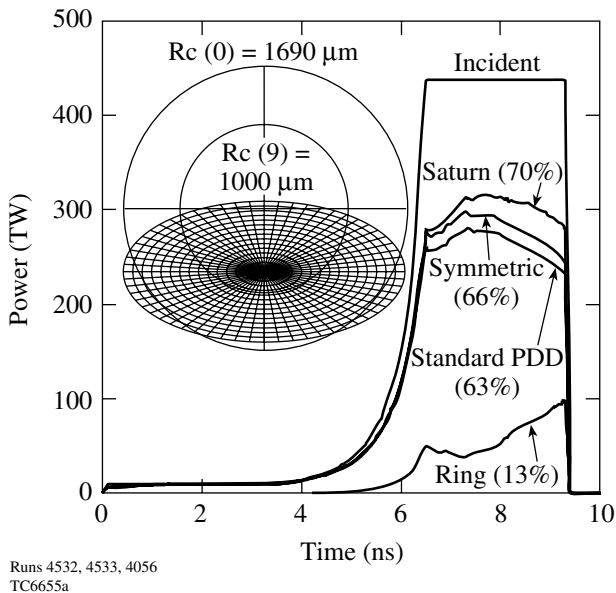


FIG. 2. Incident and capsule-absorbed laser power as a function of time for three cases: symmetric, standard PDD, and Saturn. The bottom curve applies to the ring of the Saturn target. The time-integrated absorption fractions are given in parentheses. Inset: The critical surface of the capsule at 0 and 9 ns (radii $R_c = 1690$ and $1000 \mu\text{m}$, respectively) viewed along the axis of the Ring-4 beam for the standard-PDD design, together with the elliptical far field (out to the 10% intensity contour) centered $750 \mu\text{m}$ below the target center. The grid indicates starting points for the simulation ray trace.

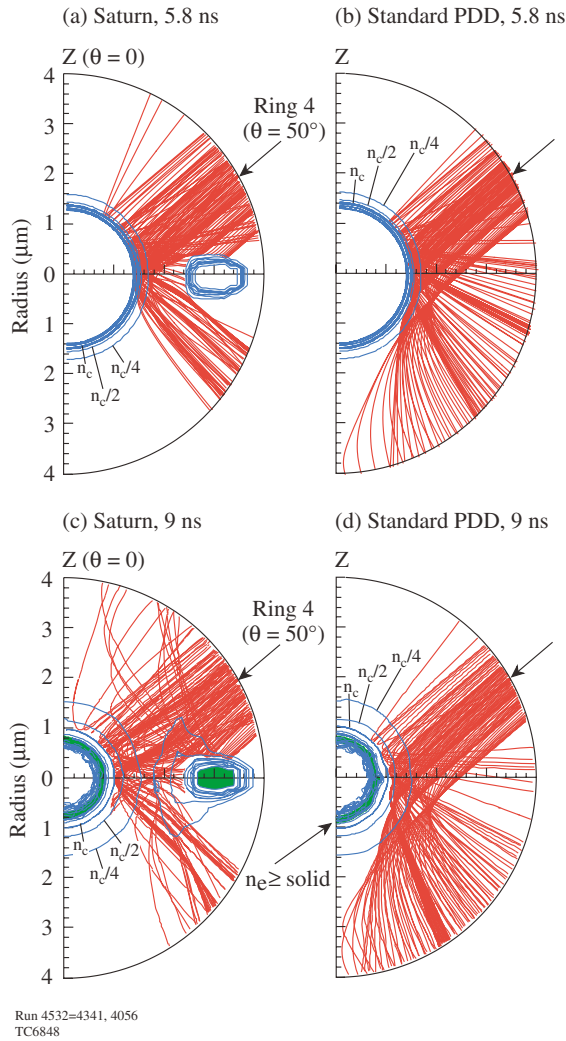


FIG. 3 (color). Electron-density contours (blue) and a representative subset of Ring-4 ray trajectories projected into the (r, z) plane (red) for a Saturn target and a standard-PDD target, at the time of shock breakout (5.8 ns) and at the end of the laser pulse (9 ns). In the Saturn design the central group of rays refract in the ring plasma at the later time (c) toward the capsule equator. The green-shaded areas at 9 ns represent material above solid density.

[9]. Figure 4 also shows that the DT shell in the Saturn case moves approximately the same distance and acquires the same velocity as for the symmetric target, indicating (consistently with Fig. 2) that there is no energy penalty associated with the Saturn design even though the laser energy, incident more obliquely, is on average absorbed further from the critical surface.

The standard-PDD pointings provide excessive drive on the equator at early times to compensate for the reduced drive at later times. This produces increased pressure gradients and motion in the θ direction. The rms V_r is 7.2% at 5.8 ns, compared with 2.5% for Saturn, and the rms V_θ at 9 ns is 1.4×10^6 cm/s, compared with 9×10^5 cm/s ($\sim 3\%$ of V_r) for Saturn. The Saturn design thus enables slightly smaller repointings to be used for Rings 1–3 to

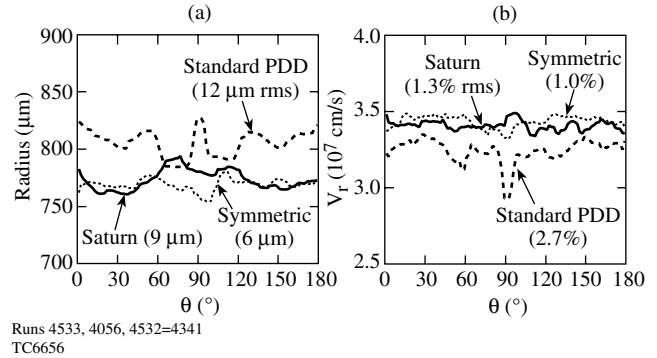


FIG. 4. (a) Center-of-mass radius and (b) radial velocity (V_r) as a function of angle θ from the vertical for the three cases—symmetric, standard PDD, and Saturn—at the end of the laser pulse (9 ns).

provide better early-time uniformity. The simulations all used a flux limiter [11] f of 0.06, broadly consistent with the observed absorption and drive in current OMEGA experiments [12]. The parameters Δr and θ_{pp} needed to optimize the PDD designs are insensitive to f .

Some simulation results of the parametric sensitivities of the designs are shown in Fig. 5, which gives the rms center-of-mass radius (ΔR_{rms}) and velocity (ΔV_{rms}) variations as functions of the pointing error of the most sensitive laser ring for all three cases and as functions of R_{major} for the Saturn design. As in Fig. 4, the Saturn performance is close to that of the symmetric case. The NIF single-beam pointing tolerance of 50 μm rms [13] should be adequate in all cases, especially as the calculations make the pessimistic assumption that all beams in the ring are displaced in unison. Figs. 5(c) and 5(d) point to an optimum R_{major} of $3100 \pm 100 \mu\text{m}$. As the ring is moved away from the capsule, ΔV_{rms} increases because fewer rays intersect the ring plasma. As the ring is moved toward the capsule, ΔV_{rms} increases dramatically due to the capsule equator becoming shadowed by the ring. Adjustment of the ring parameters provides a means for tuning the time-dependent drive symmetry of different capsule designs. Such tuning may also be required because the ring plasma, whose rate of formation depends in part on the energy near the beam edges, may evolve differently than predicted here.

From other sensitivity studies, the positioning tolerances of (a) the capsule with respect to the target chamber center and (b) the CH ring with respect to the capsule in the z direction are critical: preliminary results suggest that these should each be less than 50 μm , preferably by a factor of 2. Capsule mounting schemes taking advantage of the Saturn design must provide accurate centering of the capsule within the ring.

The optimization process that led to the Saturn design started with the investigation of target-plane profiles of the form $I(r) \propto \exp(-(r/r_0)^n)$ for the symmetric case. Obtaining a smooth overlap of deposited energy profiles from neighboring laser rings for all critical-surface radii

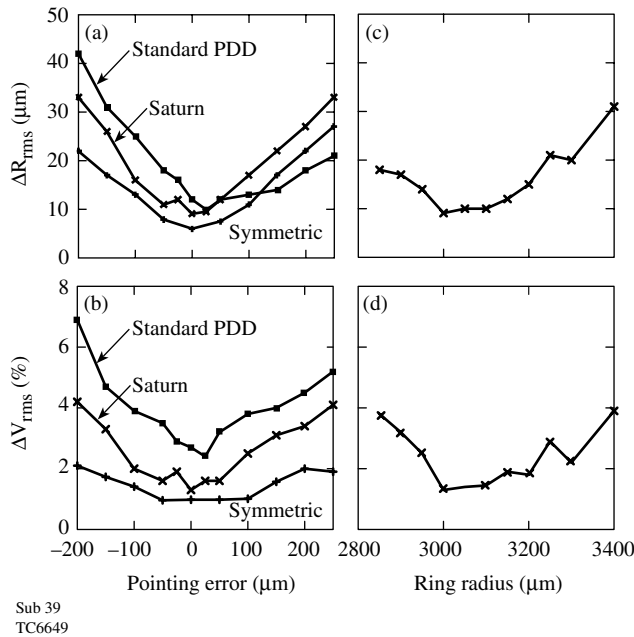


FIG. 5. Dependence of (a) the rms center-of-mass radius variation ΔR_{rms} and (b) the rms radial velocity variation ΔV_{rms} at 9 ns on the pointing error of the ring of beams with the greatest sensitivity (Ring 2 for the symmetric case, Ring 4 for the others). The same quantities are plotted against the low-Z ring major radius in (c) and (d) for the Saturn design. Each symbol corresponds to a 2D simulation, the thin lines serving only to guide the eye.

between the initial and final becomes hard when n increases above 2.5, as the edge of the profile steepens. For smaller n , an energy penalty results from rays near the edge of the beam missing the target. For $r_0 < 1200 \mu\text{m}$, non-uniformities result from the deposition being too localized, while for larger r_0 , the uniformity remains good but energy is lost. For the PDD designs, the same n and r_0 are used on the assumption that this will provide comparable azimuthal uniformity to the symmetric case. The values of Δr and θ_{pp} are chosen to spread the deposited laser energy as uniformly as possible around the capsule surface. The CH-ring parameters are chosen on the basis of surveys such as shown in Fig. 5.

Experimental investigations of PDD on the OMEGA laser system and extended simulations of the Saturn design to examine the implosion physics beyond the end of the laser pulse are underway, with preliminary results [14] demonstrating that the Saturn ring does indeed increase the drive on the equator. Issues for future investigation include characterization of the evolution and azimuthal symmetry of the Saturn ring plasma.

In conclusion, the Saturn concept will enable direct-drive implosions to be carried out on the NIF, using only the indirect-drive ports, with a uniformity approaching that of the symmetric configuration. A low-Z ring placed around the capsule provides time-dependent correction of critical laser ray trajectories to ensure adequate drive on the capsule equator at all times. Preliminary parameter surveys indicate that the tolerances necessary to ensure this high level of uniformity are reasonable. The prospects for an early ignition demonstration on the NIF using direct drive are thus greatly enhanced. Future work will calculate the gain that can be expected from these targets.

This work was supported by the U.S. Department of Energy Office of Inertial Confinement Fusion under Cooperative Agreement No. DE-FC52-92SF19460, the University of Rochester, and the New York State Energy Research and Development Authority. The support of DOE does not constitute an endorsement by DOE of the views expressed in this article.

*Electronic address: sra@lle.rochester.edu

- [1] E. M. Campbell and W. J. Hogan, *Plasma Phys. Controlled Fusion* **41**, B39 (1999).
- [2] J. Nuckolls *et al.*, *Nature (London)* **239**, 139 (1972).
- [3] J. D. Lindl, *Inertial Confinement Fusion: The Quest for Ignition and Energy Gain Using Indirect Drive* (Springer-Verlag, New York, 1998), Chap. 6, p. 61.
- [4] D. Eimerl *et al.*, in *First Annual International Conference on Solid State Lasers for Application to Inertial Confinement Fusion*, edited by M. André and H. T. Powell (SPIE, Bellingham, WA, 1995), Vol. 2633, p. 170.
- [5] S. Skupsky *et al.*, *Phys. Plasmas* **11**, 2763 (2004).
- [6] R. S. Craxton, "Two-Dimensional SAGE Simulations of Polar Direct Drive on the NIF," presented at the 33rd Anomalous Absorption Conference, Lake Placid, NY, June 2003 (Paper No. WO3).
- [7] R. S. Craxton, *Bull. Am. Phys. Soc.* **48**, 56 (2003).
- [8] C. P. Verdon, *Bull. Am. Phys. Soc.* **38**, 2010 (1993).
- [9] P. W. McKenty *et al.*, *Phys. Plasmas* **8**, 2315 (2001).
- [10] R. S. Craxton and R. L. McCrory, *J. Appl. Phys.* **56**, 108 (1984).
- [11] R. C. Malone, R. L. McCrory, and R. L. Morse, *Phys. Rev. Lett.* **34**, 721 (1975).
- [12] J. A. Delettrez, Laboratory for Laser Energetics, (private communication).
- [13] R. A. Zacharias *et al.*, in *Optical Engineering at the Lawrence Livermore National Laboratory II: The National Ignition Facility*, edited by M. A. Lane and C. R. Wuest (SPIE, Bellingham, WA, 2004), Vol. 5341, p. 168.
- [14] R. S. Craxton *et al.*, "Polar-Direct Drive—Proof-of-Principle Experiments on OMEGA and Prospects for Ignition on the NIF" (to be published).